www.springer.com/41230
https://doi.org/10.1007/s41230-022-1105-3
Research & Development
Vol. 19 No. 1 January 2022
CHINA FOUNDRY

Regulative effect of Mg/Si ratio on microstructure evolution and mechanical properties of cast Al-Li-Mg-Si alloys

Xue-jian Zhang[1], Hong-wei Wang[1], Feng-bai Ye[2], **Chun-ming Zou[1], and *Zun-jie Wei[1]

1. National Key Laboratory for Precision Hot Processing of Metals, Harbin Institute of Technology, Harbin 150001, China

2. Shanxi Pingyang Industry Machinery Co., Ltd., Pingyang 030000, Shanxi, China

Abstract: The effect of the Mg/Si ratio of Al-2.5Li-1Cu-0.8Mg-0.8Si, Al-2.5Li-1Cu-1.6Mg-0.8Si, and Al-2.5Li-1Cu-2.4Mg-0.8Si alloys on the microstructure evolution and mechanical properties was investigated. The results show that the primary phases and their morphologies in the as-cast alloys are found to vary with the Mg/Si ratio. The improvement of Mg/Si ratio of as-cast alloys promotes the formation of Mg_2Si primary phase at the expense of the AlLiSi primary phase. Moreover, a tiny amount of T_B-$Al_{7.5}Cu_4Li$ phase transforms into S-Al_2CuMg phase with the increase of Mg content. In addition, the increase of Mg/Si ratio also causes the Cu-rich intergranular phase distributed along crystal boundary to Si-rich intergranular phase. After ageing treatment, the precipitation sequence as a function of Mg/Si ratio is as follows: δ/δ'+AlLiSi (Mg/Si is ~1) → δ/δ'+β'-Mg_2Si+AlLiSi (Mg/Si is ~2) → δ/δ'+β'-Mg_2Si (Mg/Si is ~3). A good combination of strength and ductility can be obtained in Al-2.5Li-1Cu-2.4Mg-0.8Si alloy after solution and ageing. The rod-like β'-Mg_2Si precipitate has a positive influence on the comprehensive mechanical properties of the alloy.

Keywords: Mg/Si ratio; cast Al-Li-Mg-Si alloy; microstructure evolution; mechanical properties

CLC numbers: TG146.21 **Document code:** A **Article ID:** 1672-6421(2022)01-081-08

1 Introduction

Al-Li-Mg-Si alloys have achieved considerable importance due to their moderate strength, low density, excellent formability and corrosion resistance [1-5]. Nowadays, many researchers suspect that the Al-Li-Mg-Si system alloys are not only can used as wrought Al alloys, but also possibly suitable as cast Al alloys. Research shows that Mg element can be given the superior formability to the Al-Si alloys. Also, it has been found that the addition of Si element greatly affects the stress corrosion cracking resistance of the Al-Mg alloys.

Moreover, it is reported that the precipitate sequence of Al-Li-Mg-Si alloy is strongly related to the ratio of Mg and Si elements, which has a profound influence on the mechanical properties of the alloy. As for the alloy with fixed Li content, the precipitation of AlLiSi phase would be suppressed by the precipitation of β'-Mg_2Si with the Mg/Si ratio increasing from 1.8/0.8 to 2.5/0.8 [4], which coincided with the phase diagram calculated with the CALPHAD approach by Chen et al [6]. Moreover, a dual-phase δ/δ'+Mg_2Si region of the alloy may be extended within the range of the Li content from 0.5wt.% to 3.0wt.%, but it would not affect the precipitation sequence of the alloy. Mørtsell et al. [7] speculated that a large addition amount of Li (3.0wt.%) promoted the precipitation of AlLiSi and AlLi phases in lean Al-Li-Mg-Si alloys, while the β'-Mg_2Si precipitates were inhibited by the precipitation of δ'-Al_3Li phase, unless the Mg content was increased again. With the increasing of Si content (i.e., hypo-eutectic Al-8.5Si alloy), the eutectic silicon and α-Al were the main phases in the rolled A380 alloy, and the addition of Li was used as a modifier to make the eutectic Si morphology change from disk to fiber, while the secondary dendrite arm spacing of primary Al decreased with the increase of Li content, thus strengthening the mechanical properties of the alloy [3]. The addition of Cu complicated the precipitation sequence of the wrought Al-Li-Mg-Si

***Zun-jie Wei**

Ph. D., Professor, Secretary General of Heilongjiang Province Foundry Association. His research interests mainly focus on the solidification theory of nonferrous alloys (Al-base, Mg-base and TiAl alloys) under high pressure, and structural superalloys (Ti-base and Ni-base alloys) advanced casting processes.

E-mail: weizj@hit.edu.cn

****Chun-ming Zou**

E-mail: zouchunming1977@163.com

Received: 2021-05-22; Accepted: 2021-12-20

alloys, and the precipitation sequence was as follows [8-11]: supersaturated solid solution → atomic clusters → G.P. zones (pre-β") → β", L, S, C, QP, QC → β', Q'.

To date, the research works are focused on the microstructure, texture, and mechanical properties of wrought Al-Li-Mg-Si alloys [7, 8], but few studies are found concerning microstructure and mechanical performances of the cast Al-Li-Mg-Si alloys. In addition, there is insufficient data to completely understand the regulative effect of Mg/Si ratio on the microstructure evolution and mechanical performance of the alloys. In this study, cast Al-Li-Mg-Si alloys with various Mg/Si ratio were designed to investigate the effects of Mg/Si ratios on the microstructure evolution and mechanical properties of the alloys, providing theory foundation and the implementation basis for the development of a new generation of lightweight and high strength cast Al-Li-Mg-Si alloy.

2 Experimental procedure

Systematic Mg/Si ratio of the alloys was designed and subsequently prepared by conventional casting method. Pure metal Al, Al-20wt.%Si, Al-40wt.%Cu and Al-5wt.%Zr master alloys were melted in an electric resistance furnace at 750 °C. After 2 h holding, the pure Mg and Li were added into the melt under argon atmosphere, respectively. After the alloy was completely melted, 0.6wt.% C_2Cl_6 was used for degassing at 740 °C for 10 min. To ensure the complete homogenization distribution of alloying elements, the melt was discontinuously stirred at 740 °C (the interval was 15 min), kept for 90 min and then dropped down to 720 °C. In the end, the melt was isothermally held at 720 °C for about 1 h and poured into the mold pre-heated at 200 °C. Precise temperature control is a key factor in the success of remelting experiment. To ensure a stable and exact experiment process, the K-type thermocouples (Tolerance values is 0.004·|T|) with 0.5 mm external diameter was used to directly measure the temperature of the melt. The physical map, schematic diagram of the casting experiment and the size of casting are given in Fig. 1, respectively.

The chemical compositions of the alloys were conducted by Inductively Couple Plasma-Atomic Emission Spectroscopy and the results are listed in Table 1. Also listed in Table 1 are the heat treatment process parameters of the alloys, which were established by using differential scanning calorimeter (DSC) results. The as-cast alloys were subjected to heat treatments as following steps: a two-stage solution treatment in an electrical oven, and then quenched into cold water (as-quenched). Subsequently, the ageing treatment was conducted at 175 °C for 16 h in oil bath.

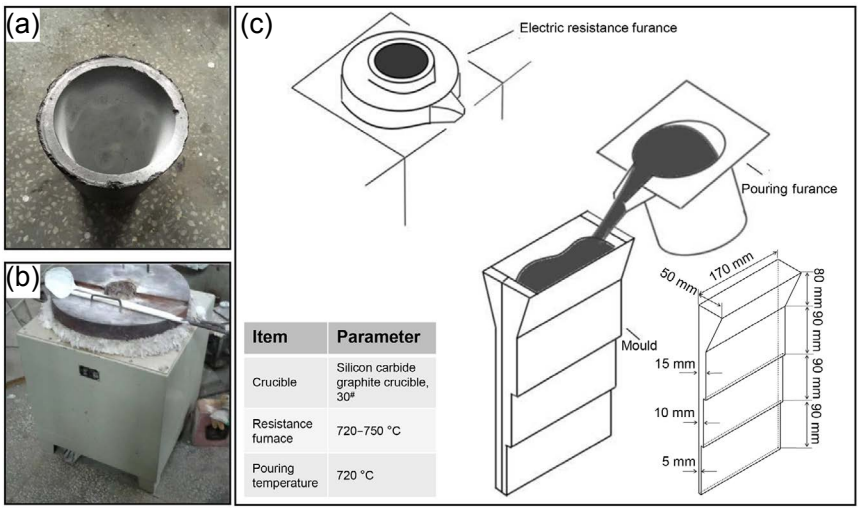

Fig. 1: Physical map of crucible (a) and resistance furnace (b), and schematic diagram of casting experiment combined with castings' dimensions and experimental parameters

Table 1: Composition of Al-Li-Mg-Si alloys given in wt.% and corresponding heat treatment process parameters

Alloy	Li	Mg	Si	Cu	Zr	Mg/Si	Solid solution	Ageing
Alloy A	2.38	0.79	0.71	0.48	0.16	~1	380 °C/16 h + 520 °C/8 h	
Alloy B	2.46	1.64	0.82	0.52	0.11	~2	350 °C/16 h + 490 °C/8 h	175 °C/16 h
Alloy C	2.57	2.47	0.85	0.44	0.13	~3	380 °C/16 h + 520 °C/8 h	

The solidification process of the studied alloys was obtained by the thermodynamic calculation software (JMatPro). All metallographic specimens were cut 5 mm above the bottom of the ingots, and then mechanically ground and etched by standard procedure using Keller's reagent for 20 s. The microstructure was observed by a FEI Quanta 200FEG Carl scanning electron microscope (SEM) with energy disperse spectroscopy (EDS). Multi-function X-ray diffraction (XRD) was used to identify the phase constitution. The tensile test was carried out by an AG-X Plus 250 kN/50 kN testing machine

with a strain rate of 0.5 mm·min^{-1}. Three specimens were tested for each alloy. Transmission electron microscopy (TEM) samples were prepared by traditional mechanical grinding and ion-thinning using a GATAN 695 precision ion-polishing system, and were analyzed by a Talos F200X transmission electron microscope (TEM) with 20 kV voltage.

3 Results

3.1 Effect of Mg/Si ratio on microstructure of as-cast and as-quenched Al-Li-Mg-Si alloys

Figures 2(a1–a3) and (b1–b2) exhibit profiles of the amount of each phase evolution as a function of temperature, XRD and DSC results corresponding to the as-cast Alloys A–C, respectively. Figures 2(a1–a3) reveal that the equilibrium AlLi phase is the dominant phase in all the three alloys due to the highest fraction of Li. Meanwhile, AlLiSi primary phase is formed in preference to Mg_2Si primary phase. Subsequently, tiny amounts of T_1-Al_2CuLi and T_B-$Al_{7.5}Cu_4Li$ phases begin to generate at 350–400 °C in Alloys A and B. With further increase of the Mg content, a tiny amount of T_B-$Al_{7.5}Cu_4Li$ primary phase will evolve into S-Al_2CuMg primary phase in Alloy C. The above results are consistent with previous research [6]. Moreover, it can be seen in Figs. 2(a1–a3) and (b1) that the primary AlLiSi phase is gradually replaced by Mg_2Si phase. As can be seen in Fig. 2(b2), there are three exothermic peaks in the DSC curves, which are corresponding to the dissolution of the AlLi equilibrium phase, AlLiSi and Mg_2Si primary phase, respectively.

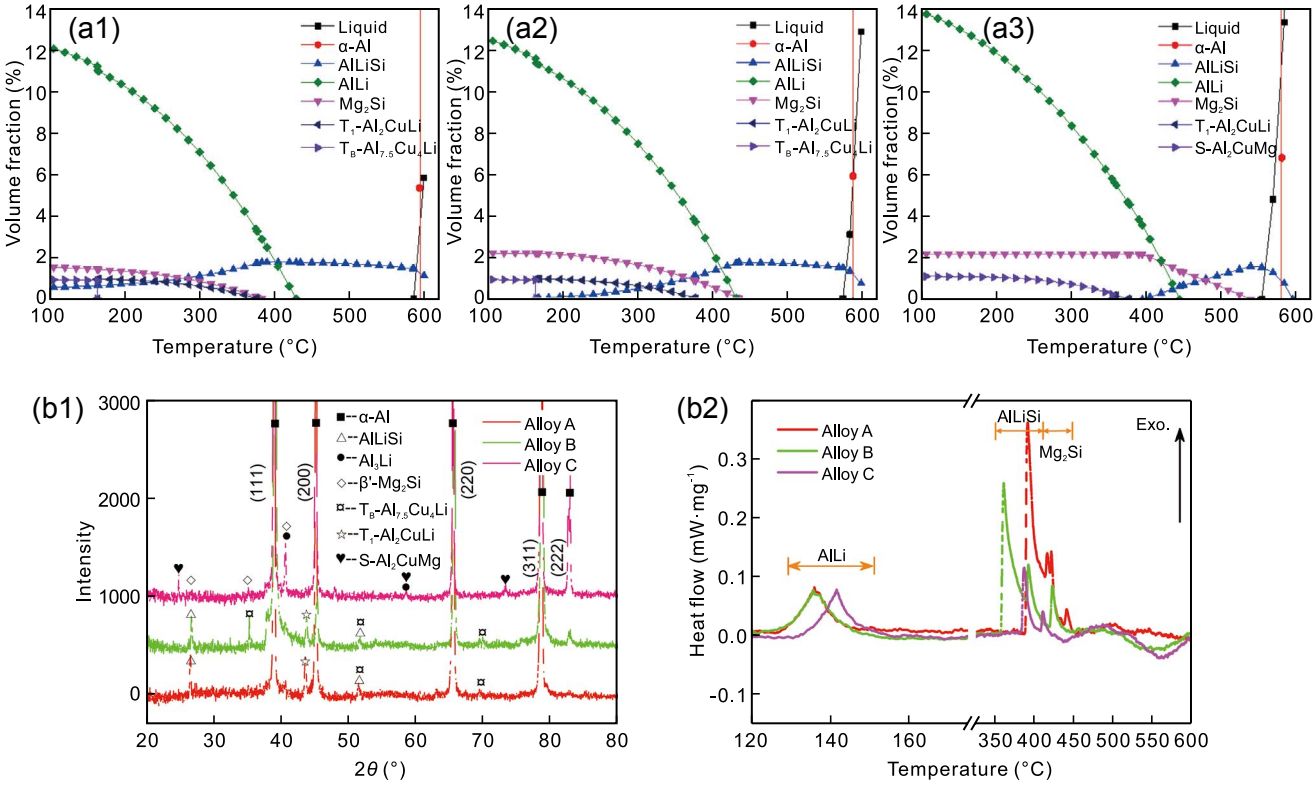

Fig. 2: Solidification process of three as-cast alloys (a1–a3), XRD patterns (b1) and DSC curves (b2)

Figures 3(a1–a3) and (b1–b3) illustrate the SEM-EDS images of Alloys A–C in as-cast and as-quenched state, and the corresponding EDS results are also given. In Alloy A, Cu atoms will be pushed to the forefront of the liquid-solid interface during the solidification process, which eventually will form intergranular Cu-rich phases along the grain boundaries at the end of solidification [as can be seen in Fig. 3(a1)] due to the low equilibrium distribution coefficient of Cu (K_{Cu}=0.17 [12]). Figures 3(a1–a3) and the EDS results show that the coarse second phases, including white Cu-rich particles and grey Si-rich intermetallics, distribute along the crystal boundaries in all three alloys. With the increase of Mg content, Mg participates in the formation of the Cu-rich particles, and the globular-like intermetallics evolve into alphabet-like. When increasing the Mg/Si ratio, corresponding to Alloys B and C, the Mg concentration in the melt exceeds the threshold solid solubility of liquid-solid interface under non-equilibrium solidification conditions. Consequently, excessive "Mg-Si" clusters will also be pushed by liquid-solid interface, and finally forming the intergranular Si-rich phases, as can be seen in Figs. 3(a2) and (a3). The SEM microstructures of the as-quenched alloys are displayed in Figs. 3(b1–b3), respectively. After solution, most of the Cu-rich intermetallic compounds in the as-cast alloy dissolve into the α-Al matrix, with the exception of a few small residual Si-rich intermetallics along the grain boundaries, which can be attributed to the extremely high melting point of Si-containing compounds [13].

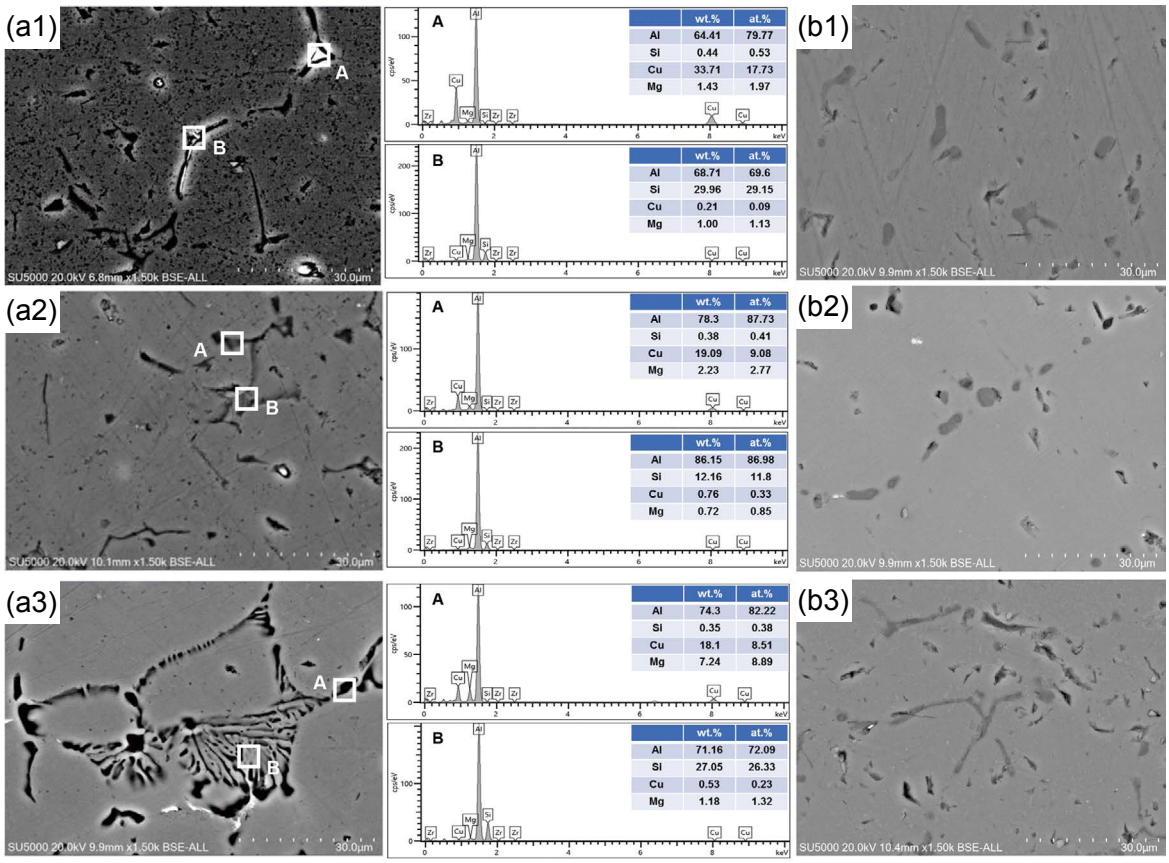

Fig. 3: SEM-BSE patterns of microstructure of three alloys in as-cast (a1–a3) and as-quenched (b1–b3), respectively

3.2 Effect of Mg/Si ratio on microstructure of Al-Li-Mg-Si alloys after solution and ageing treatment

Ageing treatment might induce the precipitation of nano-scale precipitates within α-Al matrix, while having no significant effect on the micron-scale intergranular phase of as-quenched alloys. In order to further understand the relationship between ageing microstructure and Mg/Si ratio of the studied alloy during artificial ageing, TEM was applied to observe the microstructures of Alloys A–C under artificial ageing at 175 °C for 16 h, as shown in Fig. 4. Figure 4(a1) shows that two main kinds of spherical-like nano-precipitates, including δ'-Al_3Li and AlLiSi particles, are embedded in the α-Al matrix of the Alloy A, which can be identified by the corresponding Fourier transform patterns (FFT) in Figs. 4(a3) and (a4). Figures 4(b1–b4) and (c1–c4) show that the increase of Mg/Si ratio causes the transformation of AlLiSi particles into the rod-like β'-Mg_2Si precipitates, while the coarsening of β'-Mg_2Si precipitates combined with the negligible change of precipitation density will occur with increased Mg content of alloy.

As can be seen in Fig. 4, Mg content increase will significantly promote the precipitation of β'-Mg_2Si precipitates and inhibit the formation of AlLiSi particles; that is to say, rod-like β'-Mg_2Si precipitates are formed in preference to AlLiSi particles with the increase of Mg content. Mg has high binding energy with vacancies (0.25±0.03 eV) [14]. The formation of "Mg-vacancy" clusters will be promoted with the increase of Mg content in the alloy, which offers sufficient driving force for the precipitation of β'-Mg_2Si precipitates. Compared with Alloy A, therefore, the number of β'-Mg_2Si precipitates in the Alloys B and C is significantly increased. Moreover, the rod-like β'-Mg_2Si precipitates keep on growing with the increase of Mg content, as shown in Figs. 4(b3) and (c3). The length of the rod-like β'-Mg_2Si precipitates increases from ~15 nm to ~40 nm, while the diameter only increases to 3.18 nm from 2.32 nm. It's worth noting that the inverse Fourier transform spectrum in Fig. 4(c4) shows that twining structure forms in the grown rod-like β'-Mg_2Si precipitates with a coherent relationship with the matrix, which makes the β'-Mg_2Si precipitates difficult to be sheared by dislocations.

3.3 Effect of Mg/Si ratio on mechanical properties and fracture mode of cast Al-Li-Mg-Si alloys

Figure 5(a) shows the true tensile stress-strain curve of Alloys A–C after solution and ageing treatment and the representative fracture morphologies are presented in Figs. 5(b–d), respectively. Compared with Alloy A (Mg/Si is ~1), as shown in Fig. 5(a), the yield strength (YS), ultimate tensile strength (UTS) and elongation (EL) are respectively increased from 242.7±7.5 MPa to 261.2±9.4 MPa, 331.7±4.7 MPa to 360.9±10.3 MPa and (8.82±0.51)% to (12.67±2.8)% with Mg/Si ratio increases to ~2 (Alloy B). A good combination of strength (YS=278.6±11.4 MPa, UTS=374.3±12.6 MPa) to ductility (EL=14.74%±2.1%) can be obtained in Alloy C with the highest Mg/Si ratio in this study.

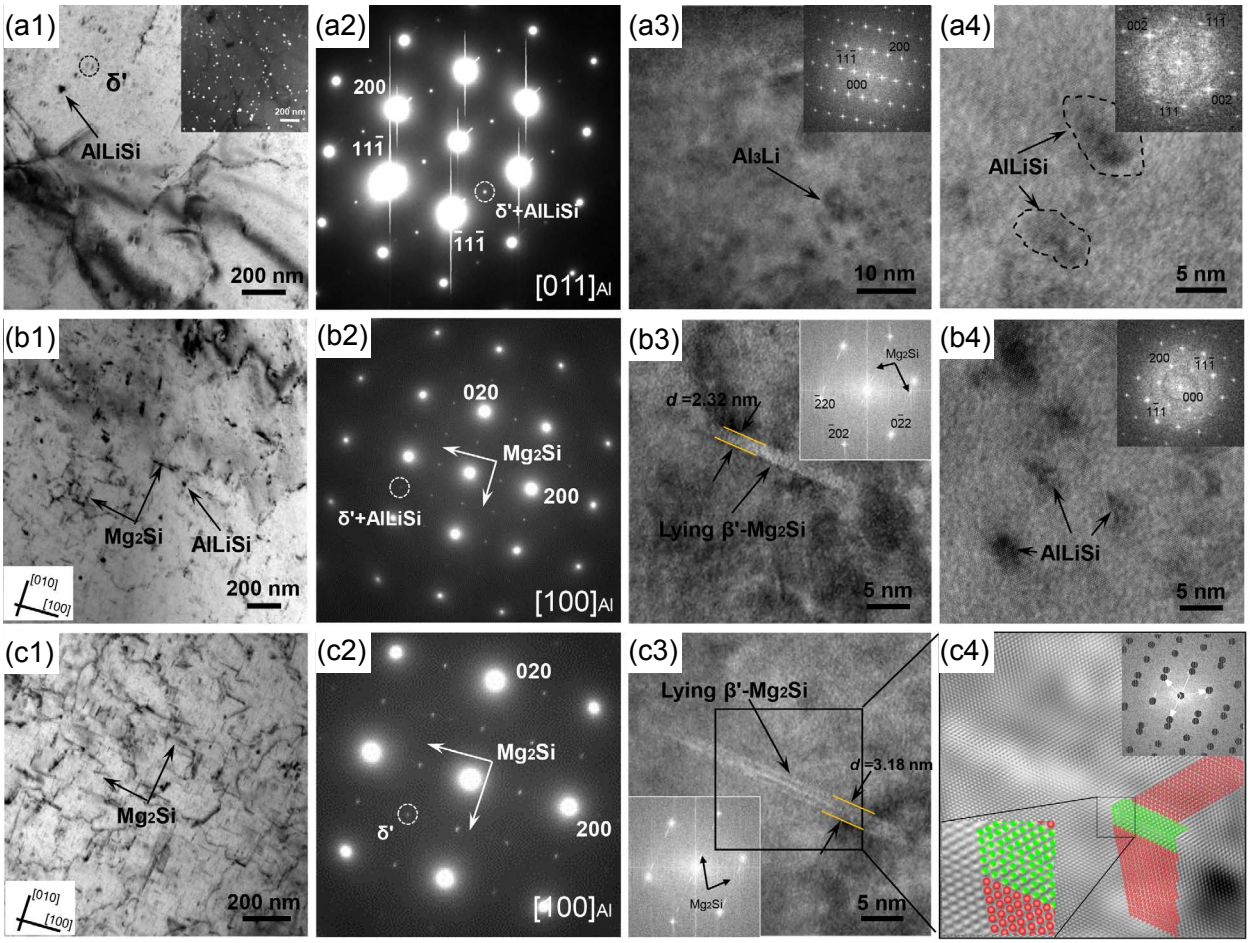

Fig. 4: Microstructure of all three aged alloys: (a1) TEM BF (bright field) image of Alloy A and corresponding center dark field image (inset) viewed near <011>$_{Al}$; (a2) corresponding SAD (selected area diffraction) of Alloy A; (a3) and (a4) high resolution pattern and corresponding Fourier transform spectrum (inset) of δ'-Al_3Li and AlLiSi particles embedded in Alloy A, respectively; (b1–b4) and (c1–c4) BF images, diffraction patterns and corresponding Fourier transform spectrum of Alloys B and C (B=[100]$_{Al}$), respectively; (c4) inverse Fourier transform spectrum of rod-like β'-Mg_2Si precipitates

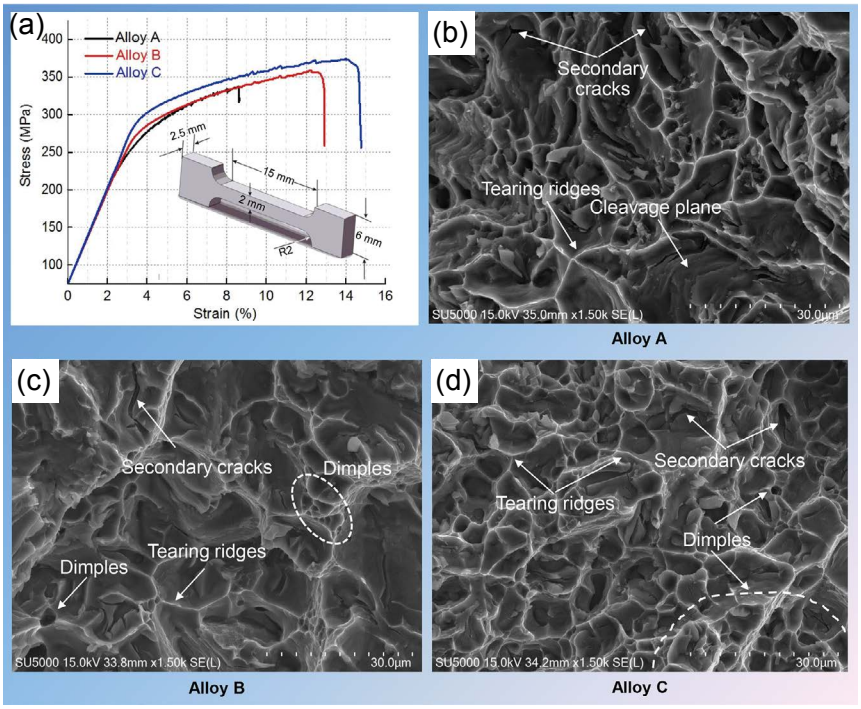

Fig. 5: True tensile stress-strain curve of three alloys of solution and ageing at ambient temperature and dimensions of dog-bone shaped samples for tensile testing are also shown (a), and fracture morphologies of Alloys A–C (b–d), respectively

As is known, the mechanical performance of cast Al-Li alloys, as typical precipitation strengthening aluminum alloys, is directly related to their microstructure. The improvement of strength can be mainly attributed to the increase of rod-like β'-Mg_2Si precipitates. The relationship between strengthening and the shape of precipitates conforms to the following expressions [15]:

$$\Delta\sigma = 0.81\frac{G\boldsymbol{b}}{2\pi(1-\nu)^{1/2}}\left(\frac{\ln(d/\boldsymbol{b})}{0.615d(2\pi/3f)^{1/2}-d}\right) \quad (1)$$

where, G and ν are the shear modulus and Poisson's ratio of Al matrix, respectively. Moreover, f and d are the volume fraction and diameter of the precipitates. And $\boldsymbol{b}$ is the Burgers vector of edge dislocation in Al alloy ($\boldsymbol{b}$=1/2<110> in FCC metal [16]). In this study, it is assumed that this equation is a valid approximation for β'-Mg_2Si strengthening and take d as the diameter of the β'-Mg_2Si rods. Thus, it can be seen that the relationship between the strengthening of alloys and the diameter/volume fraction of precipitates is nonlinearly conformable. Therefore, the increase of diameter/volume fraction of rod-like β'-Mg_2Si precipitates results from the increase of Mg/Si ratio, improving the property of alloys.

As can be seen in Fig. 5(a), the tensile curve of Alloy A shows relatively low strength and elongation, while the tensile curves of Alloys B and C exhibit a good combination of strength and ductility. Figure 5(b) shows the fracture morphology of Alloy A, which exhibits the quasi-cleavage fracture mode. The fracture surface of Alloy A includes a large number of tearing ridges and secondary cracks combined with cleavage plane, illustrating the typical quasi-cleavage fracture mode, which corresponds to the poor mechanical properties of Alloy A. Apart from the above fracture features, however, a number of dimples can also be observed on the fracture morphology of Alloys B and C, corresponding to Figs. 5(c) and (d). Moreover, Figs. 5(c) and (d) also show that the number of dimples on the fracture morphology of Alloys B and C increases gradually with the increase of Mg/Si ratio. Comparing the fracture morphology of these three alloys, it can be inferred that the Mg/Si ratio of alloy has a profound impact on the toughening behavior.

4 Discussion

To illustrate the effect of the Mg/Si ratio on the mechanical properties and fracture mode of alloys, the fracture behavior of three alloys is discussed in detail below. Take Alloy A for example, it can be observed in the dark field image in Fig. 4(a1) that a large number of δ'-Al_3Li particles embed within the matrix (the existence of δ'-Al_3Li particles in the other two alloys can also be identified by the superlattice reflections in the SAD patterns in Figs. 4(b2) and (c2), respectively). The δ'-Al_3Li particles have a cubic structure with a lattice parameter of a=0.405 nm, which maintains a coherent relationship with matrix [16]. Its nucleation and growth mechanisms are usually followed by the spinodal decomposition process and classical Lifshitz-Slyozov-Wagner (LSW) growth theory. The acceptable strengthening mechanism of δ'-Al_3Li is dislocation cutting mechanism [17]. In general, the δ'-Al_3Li particles, as a typical strengthening phase in Al-Li system alloys, can effectively increase the specific elastic modulus and specific strength of alloys. However, the planar slip of the δ'-Al_3Li particles will intensify the intergranular brittle fracture tendency [18]. As above, a large number of δ'-Al_3Li particles in Alloy A aggravate the brittle quasi-cleavage fractures tendency, which causes Alloy A to display poor mechanical properties. Moreover, the brittle AlLiSi particles, which are commonly considered to be harmful for the ductility of Al-Li-Mg-Si alloys, are also detected in Figs. 4(a4) and (b4). The aforementioned particles combined with rod-like β'-Mg_2Si precipitates are considered to be beneficial to the strength of Al-Li-Mg-Si alloys, however, the local stress concentration will be increased in a certain degree. Wang et al. [19] indicated that increase of the Cu content in Al-Si alloys deteriorated the ductility significantly. The fracture behavior of Al-Si alloys with high Cu content was predominantly influenced by the brittle Al_2Cu phase rather than by the Si particles. The initiation of crack occurred by the breaking of the intermetallic, rather than by destroying the boundaries among the intermetallic or the boundaries between the intermetallic phases and the α-Al matrix. Zhang et al. [20] also reported that the predominate reason for the brittle fracture in Al-Si piston alloy cannot be attributed to the debonding or the fracturing of Si platelets. Figure 6(a) presents the distribution of Cu-rich intermetallics on the fracture surface of Alloy A, which proves that the cracks propagate along these Cu-rich intermetallics. These Cu atoms will bond with Mg to form Mg-Cu intermetallics with lower melting point in the Alloys B and C with higher Mg content, and then dissolve back into the matrix. As can be seen from the schematic diagram in Fig. 6(b), the local stress concentration generates in Alloy A under uniaxial tensile load. The stress concentration promotes the initiation of cracks within the Cu-rich compounds with poor deformability rather than the interface between the compounds and matrix. Subsequently, the cracks propagate inside the compounds. And then, when the cracks develop to the matrix, the propagation of the full growth cracks can no longer be hindered by matrix, which results in the poor mechanical properties of Alloy A.

However, the rod-like β'-Mg_2Si precipitates in Alloys B and C can be used to toughen aluminum alloys by inhibiting dislocation movement. The STEM-BF (bright image) patterns in Fig. 6(c) shows the dislocations pile up at the interface of rod-like β'-Mg_2Si precipitates/α-Al matrix in artificially aged Alloy B. It can be seen that the dislocations have piled up around the rod-like β'-Mg_2Si precipitates, which implies that the rod-like β'-Mg_2Si precipitates can effectively alleviate the local stress concentration. The existence of the rod-like β'-Mg_2Si phases weakens the local stress concentration by hindering dislocations movement, which makes the fracture cracks hard to initiate and spread within the intermetallics [Fig. 6(b)]. In summary, in the Alloys B and C with higher

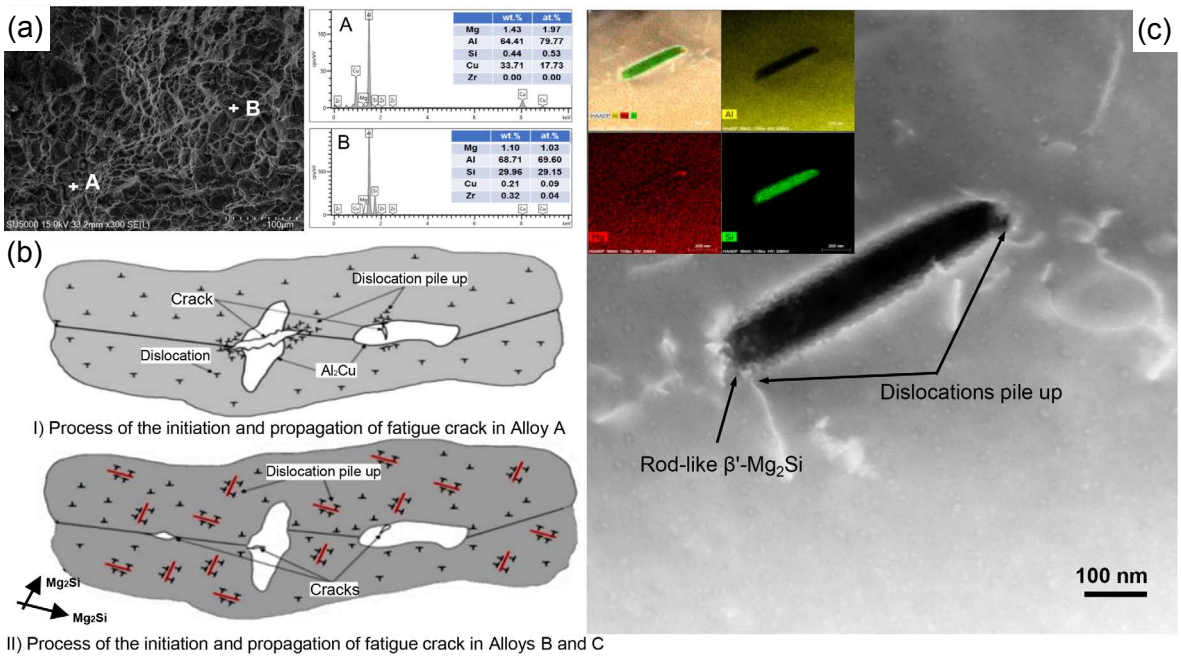

Fig. 6: Fracture morphology and corresponding EDS results of Alloy A which indicates the distribution of Si-, Mg-rich particles and Al_2Cu phase (a), schematic illustration of influence of rod-like β'-Mg_2Si precipitates on process of initiation and propagation of fatigue cracks (b), and STEM-BF (bright image) patterns of dislocations pile up at interface of rod-like β'-Mg_2Si precipitates/α-Al matrix (c)

Mg/Si ratio, on the one side, the tendency of crack source initiation is decreased by the transformation from Cu-rich compounds (in Alloy A) to Mg-, Si-rich compounds; on the other side, the precipitation of the rod-like β'-Mg_2Si precipitates can effectively alleviate the local stress concentration, thus the formation and spreading of cracks will be suppressed. These two aspects can effectively improve the comprehensive mechanical properties of Alloys B and C.

5 Conclusions

In this study, the microstructure evolution of as-cast and heat-treated Al-Li-Mg-Si alloy with various Mg/Si ratios was described, and the mechanical properties and fracture mechanism of heat-treated alloys were tested. The main conclusions are as follows:

(1) Various Mg/Si ratios result in different phase constitutions in as-cast alloys. The main primary phases are the equilibrium AlLi, Mg_2Si and AlLiSi phases. With the increasing of the Mg/Si ratio from ~1 to ~2, the formation of primary AlLiSi phase is prior to that of Mg_2Si phase during the solidification process. In the alloy with the highest Mg/Si ratio, moreover, a tiny amount of T_B-$Al_{7.5}Cu_4Li$ phase evolves into S-Al_2CuMg phase.

(2) The ageing treatment can promote the precipitation of a large number of spherical-like δ'-Al_3Li particles and AlLiSi particles, while the increase of Mg/Si ratio can promote the transformation of the spherical-like AlLiSi particles into the rod-like β'-Mg_2Si. However, the precipitation density of β'-Mg_2Si precipitates is limited by the fixed Si content in Alloy C.

(3) Tensile properties of the alloys are notably improved with the increase in the Mg/Si ratio. The UTS values of the alloys with ~1, ~2 and ~3 Mg/Si ratios are 331.7±4.7 MPa, 360.9±10.3 MPa and 374.3±12.6 MPa, with the elongations of (8.82±0.51)%, (12.67±2.8)% and (14.74±2.1)%, respectively.

(4) The precipitation of rod-like β'-Mg_2Si precipitates profoundly improves the comprehensive properties of alloys by dislocation bypass mechanism. In the alloy with Mg/Si ratio ~1, there is a lack of the sufficient amount of barriers, which can effectively block the slip of dislocations, resulting in the accumulation of dislocations at the interface of Al_2Cu intermetallics/matrix and/or grain boundary. The accumulation of dislocations causes the initiation and propagation of cracks in the intermetallics by enhancing the stress field of main crack and the alloy will soon fail. With the increasing of Mg/Si ratio, the precipitation of rod-like β'-Mg_2Si precipitates relieves the local stress concentration, which obviously improves the elongation of the alloys.

Acknowledgements

This research was financially supported by the National Natural Science Foundation of China (51774105) and Touyan Innovation Team Program (XNAUEA5640208420).

References

[1] ud-Din S, Awais H B, ul-Haq Tariq N, et al. Effect of Li addition on microstructure and mechanical properties of Al-Mg-Si alloy. International Journal of Materials Research, 2014, 105(8): 770–777.

[2] Zhao Z K, Qiao Z, Chang L L, et al. Effect of Li on Al-Si alloys structure and properties. Advanced Materials Research, 2009, 79–82: 119–122.
[3] Karamouz M, Azarbarmas M, Emamy M, et al. Microstructure, hardness and tensile properties of A380 aluminum alloy with and without Li additions. Materials Science & Engineering A, 2013, 582: 409–414.
[4] Deschamps A, Sigli C, Mourey T, et al. Experimental and modelling assessment of precipitation kinetics in an Al-Li-Mg alloy. Acta Materialia, 2012, 60(5): 1917–1928.
[5] Koshino Y, Kozuka M, Hirosawa S, et al. Comparative and complementary characterization of precipitate microstructures in Al-Mg-Si(-Li) alloys by transmission electron microscopy, energy dispersive X-ray spectroscopy and atom probe tomography. Journal of Alloys & Compounds, 2015, 622: 765–770.
[6] Chen R, Huang Z, Chen C Q, et al. Thermodynamic calculated and TEM observed microstructure of Al-Li-Mg-Si alloys. Materials Science & Engineering A, 2000, 280: 146–150.
[7] Mørtsell E A, Marioara C D, Andersen S J, et al. The effects and behaviour of Li and Cu alloying agents in lean Al-Mg-Si alloys. Journal of Alloys & Compounds, 2016, 699: 235–242.
[8] Yang X, Xiong B, Li X, et al. Microstructure characterization of as-cast Al-Mg-Si alloys with high content Li element addition. Materials Research Express, 2019, 6(11): 1165e5.
[9] Marioara C D, Andersen S J, Jansen J, et al. Atomic model for GP-zones in a 6082 Al-Mg-Si system. Acta Materialia, 2001, 49(2): 321–328.
[10] Andersen S J, Marioara C D, Vissers R, et al. The structural relation between precipitates in Al-Mg-Si alloys, the Al-matrix and diamond silicon, with emphasis on the trigonal phase U1-$MgAl_2Si_2$. Materials Science & Engineering A, 2007, 444(1–2): 157–169.
[11] Andersen S J, Marioara C D, Frøseth A, et al. Crystal structure of the orthorhombic U2-Al4Mg4Si4 precipitate in the Al-Mg-Si alloy system and its relation to the β' and β'' phases. Materials Science & Engineering A, 2005, 390(1–2): 127–138.
[12] StJohn D H, Prasad A, Easton M A, et al. The contribution of constitutional supercooling to nucleation and grain formation. Metallurgical and Materials Transactions A, 2015, 46A: 4868.
[13] Beatrice C R S, Garlipp W, Cilense M, et al. Vacancy-Mg atom binding energy in Al-Mg alloys. Scripta Metallurgica et Materialia, 1995, 32: 23–26.
[14] Schueller R D, Wawner F E, Sachdev A K. Strengthening potential of the cubic σ precipitate in Al-Cu-Mg-Si alloys. Journal of Materials Science, 1994, 29(1): 239–249.
[15] Starink M J, Wang P, Sinclair I, et al. Microstructure and strengthening of Al-Li-Cu-Mg alloys and MMCs: II. Modelling of yield strength. Acta Materialia, 1999, 47(14): 3855–3868.
[16] Wang S C, Starink M J. Precipitates and intermetallic phases in precipitation hardening Al-Cu-Mg-(Li) based alloys. International Materials Reviews, 2005, 50(4): 193–215.
[17] Kumar K S, Heubaum F H. The effect of Li content on the natural aging response of Al-Cu-Li-Mg-Ag-Zr alloys. Acta Materialia, 1997, 45(6): 2317–2327.
[18] Chen A T, Wu G H, Zhang L, et al. Microstructural characteristics and mechanical properties of cast Al-3Li-*x*Cu-0.2Zr alloy. Materials Science & Engineering A, 2016, 677: 29–40.
[19] Wang Q G, Cáceres C H. The fracture mode in Al-Si-Mg casting alloys. Materials Science & Engineering A, 1998, 241(97): 72–82.
[20] Zhang G H, Zhang J X, Li B C, et al. Characterization of tensile fracture in heavily alloyed Al-Si piston alloy. Progress in Natural Science, 2011, 21(5): 380–385.